Image Cover Sheet

CLASSIFICATION	SYSTEM NUMBER
UNCLASSIFIED	501055

TITLE

BOTTOM REFLECTION COEFFICIENT MEASUREMENT AND GEOACOUSTIC INVERSION AT THE CONTINENTAL MARGIN NEAR VANCOUVER ISLAND WITH THE AID OF SPIKING FILTERS

System Number:

Patron Number:

Requester:

Notes:

DSIS Use only:

Deliver to:

Bottom reflection coefficient measurement and geoacoustic inversion at the continental margin near Vancouver Island with the aid of spiking filters

Garry J. Heard*
Defence Research Establishment Pacific, FMO Esquimalt, B.C. Canada, V0S 1B0
(September 2, 1994)

This paper presents the results of an experiment to measure the reflection coefficient-vs-grazing angle at the continental margin west of Vancouver Island. The measured reflection coefficients are inverted and estimates of the surficial sediment geoacoustic properties obtained.

The receiver used in this experiment was a long towed-array with the source in aft-endfire aspect. The acoustic sources for this experiment were explosives that produced direct-path arrivals approximately 0.1 seconds in length. Bottom and sub-bottom arrivals continued for several seconds duration. Explosives were detonated at intervals such that bottom reflected energy received at the array sampled grazing angles in the interval 10–80°.

Source-receiver ranges were computed by measuring arrival time differences at each of the array elements, comparing these time differences with those computed using a ray-tracing propagation model, and globally minimizing the accumulated squared time difference residuals. To aid in the measurement of arrival times, spiking filters were employed to produce a *deconvolution-like* output that separates arrivals overlapped in the original time-series. The reflection coefficient estimates were determined from the linear spiking filter outputs by forming the ratio of the direct-path and bottom-reflected arrival amplitudes. This technique is efficient and provides estimates of the surficial sediment reflection coefficient by excluding energy returned from sub-bottom layers.

(*Keywords: shaping filters, reflection coefficients, bottom measurements*)

INTRODUCTION

The WEDGEX field trial was carried out using the COAMS (Canadian Oceanographic Acoustic Measurement System) [1] off the west coast of Vancouver Island to investigate low frequency propagation for upslope and downslope geometries. In order to interpret the propagation loss [2] it was necessary to estimate the geoacoustic bottom parameters in a region where the sea floor sloped almost uniformly along the track up the slope at the edge of the continental margin.

Signal Underwater Sound (SUS) charge explosives were used as the acoustic sources in this experiment. The explosion signals were received on a 32 element sub-array of the 128-channel COAMS array. The array was oriented in aft-endfire aspect to the source location such that each detonation provided data that could be used to estimate the reflection coefficient at 32 different grazing angles. In total, 11 source detonations occurred and the first eight of these were employed in this study providing 256 measurements of reflection loss-vs-grazing angle over a range of 10°–80°.

Acoustic arrival timing information was used to determine the source-receiver range. Direct measurement of the acoustic arrival times in the recorded data was made difficult by the overlap of the arrivals in the raw data. This was further complicated by the inclusion of a pre-whitening filter in the array system that tended to destroy the impulsive nature of the explosion signals. These difficulties were overcome by employing a linear filter commonly known as a 'spiking' filter. The spiking filter was developed using a standard technique and employed a sampled waveform as the 'input' that was to be converted to a short duration triangular spike of unit amplitude. The result of spiking the raw data was to produce a time-series in which acoustic arrivals appear as triangular-shaped pulses in a background of noise. The result is an approximation of the desired deconvolution of the raw data. Timing information was obtained by determining the sample that corresponded with the leading edge of each triangular spike.

Time differences between acoustic arrivals were compared with time differences calculated using a ray-tracing propagation model. The array position was determined by globally minimizing the accumulated squared residuals of

*Now at: Defence Research Establishment Atlantic, PO Box 1012 Dartmouth, NS, Canada B2Y 3Z7

the difference between measured and modelled time differences [3]. The resulting array positions were considered to be accurate to approximately 10 m.

Inspection of the spiked data records showed that sub-bottom arrivals were separable from the bottom-reflected arrivals over a large range of grazing angles. Similarly, the direct-path and surface-reflected arrivals were also separable over a large spread of source-receiver ranges. This separation of secondary arrivals implied that the amplitudes of the spikes would be a good estimate of the wavelet amplitudes by nature of the linear character of the spiking filters [4]. This fact, suggested that an estimate of the reflection coefficients could be obtained by adjusting the spiked arrival amplitudes by a factor related to the time of flight (spherical spreading) and forming the ratio of the adjusted bottom-reflected spike amplitude to the adjusted direct-path spike amplitude. The final requirement was to relate each reflection coefficient estimate to the appropriate grazing angle. This task was easily accomplished using the same ray-tracing model used earlier.

Once the reflection coefficient-vs-grazing angle estimate has been made, an estimate of the surficial sediment geoacoustic properties can be obtained by inversion. In this report, the geoacoustic properties of the sediment have been inverted using two different techniques: the first, a brute force search over allowable parameter ranges described by Chapman *et al.* [5], and the second, a simulated annealing search due to Hannay and Chapman [6]. The inversion process is somewhat similar to that which arises in matched field processing; however, the dimensionality of the inversion space is generally smaller and the forward modelling much simpler and faster in this problem than in many matched field inversion problems. Rather than trying to match field values at various receivers, which requires the use of a computationally intensive propagation model, we simply fit a reflection coefficient curve to the measured reflection curve for a simple layered bottom. Using this technique we can obtain inversion results for the surficial sediments very rapidly even on a small computer. In addition, this method is relatively insensitive to the receiving array position uncertainty that would otherwise require the use of focalization techniques [7] and an increase in the computation time. It may be that some individuals would use our technique to provide initial estimates and bounds for the surficial sediment properties to be used in a more elaborate matched field inversion scheme where *a priori* information might otherwise be minimal.

In the next section, the WEDGEX experiment and the methods that were employed to develop a suitable spiking filter for the analysis are described. Section II describes the technique used to measure the arrival times and estimate the reflection coefficient. Section III presents the geoacoustic inversion results obtained with the two techniques previously mentioned. Finally, Section IV presents conclusions and briefly summarizes the results.

In Appendix A spiking filters are described in more detail following the approach described in Robinson and Trietel [8]. Appendix B summarizes the results of a heuristic study of the uncertainties in the timing and amplitude measurements for simulated conditions similar to those encountered with the WEDGEX data set.

I. WEDGEX TRIAL AND SPIKING FILTER DESIGN

A. WEDGEX field trial

In 1987, the WEDGEX field trial was conducted at a location off the west coast of Vancouver Island. Figure 1 shows the source location, the track of the COAMS receiver, and the bathymetry.

During the trial 11 SUS (Signal Underwater Sound) charges were dropped at roughly 10-minute intervals from a stationary source ship at the location indicated, while the COAMS array was towed directly away from the source ship location up the slope of the continental margin. The SUS charges detonated at approximately 183 m and produced a broadband signal with a 6 dB bandwidth of approximately 120 Hz and a maximum source level at 50 Hz [9,10].

The COAMS array was towed at a nearly constant speed of 4 knots, at a mean depth of 221 m. The tow direction was almost directly up the slope toward the shallow water with the array in aft-endfire aspect to the source. The towed-array system provided data on a 32-element sub-array with a sampling rate of 699.05 Hz. The inter-element spacing within the array was 38.1 m providing a total aperture of 1181.1 m.

The bathymetry in the area was almost uniformly shelving from a depth of 1500 m to 450 m along the 15-km track, except in the region between the source and the early portion of the receiver track. In this particular area, a shallow canyon exists that runs parallel to the 1500 m depth contour.

The sound speed profiles were measured before, during, and after the experiment with the aid of expendable sound velocity probes (XSV). A mean sound speed profile was adopted for use with the ray-tracing model that was employed to determine the grazing angles and source-receiver ranges.

The model employed was a simple implementation of the constant-gradient ray-tracing method with the ability to handle a range-dependent bottom. The model breaks the environment into a number of layers in which the sound-speed can be approximated by a linear profile. Relatively simple numerical integrations are then performed

to calculate the time-of-flight and end-point location of the acoustic ray. A binary search is performed to find the eigenray that connects the source and receiver given a desired number of surface and bottom interactions. Corrections to the bottom interaction angles are made by looking at bottom-slope data obtained from an echo-sounder record made simultaneously with the reflection loss experiment.

B. Spiking filter design for the estimation of ocean bottom reflection coefficients

Spiking filters are well known amongst the geophysical community, but they are rarely used in underwater acoustics. The spiking filter used in this application is developed using fairly standard techniques as described by Robinson and Treitel [8]. A summary description of the technique for creating spiking filters is given in Appendix A.

For the current application of estimating ocean bottom reflection coefficients it is assumed that the acoustic energy is composed of a sum of delayed, amplitude reduced, and phase-shifted replicas of an input wavelet corresponding to the initial shock and subsequent bubble pulses of the explosive source modified by the pre-whitening filter of the receiving array system. When a properly designed spiking filter is applied to such a signal, the resulting output is a sequence of spikes (of the desired shape) that appear at times corresponding to the arrivals of the source wavelet after transmission along various isolated propagation paths. The amplitudes of the spikes are a measure of the amplitudes of the wavelet arrivals after having suffered spreading and reflection/transmission losses in the media and at boundaries. The relationship between the wavelet amplitudes and those of the resulting spikes is guaranteed by the linear nature of the spiking filters, which are implemented as simple FIR filters. The major factors that effect the performance of the spiking filter are dispersion, and the degree of wavelet overlap in the received time-series.

Geometrical dispersion is not a problem in the current work because the data is modelled as a sum of delayed, scaled multi-path arrivals and we limit the application of the filter to situations where the filter is able to separate the bottom and sub-bottom arrivals. This separation of sub-bottom energy allows us to treat the bottom as a simple half-space and allows the direct determination of the surficial sediment properties independent of frequency. Intrinsic dispersion can be ignored because absorption in the water is extremely small at the frequencies of interest (*i.e.*, 25–145 Hz). The major difficulty arises when the spiking filter is unable to resolve highly overlapped arrivals. In the current situation, this effect was observed on occasion and resulted in anomalous values of the reflection coefficient (*i.e.*, responsible for some scatter in the reflection coefficient). Fortunately, the technique was applicable to the majority of the data (the first 8 of the 11 shots) and the critical angles were observable in the applicable data. The method might not have been applicable had the critical angles been smaller than they were or if strong sub-bottom returns were observed to merge with the bottom reflected signal sooner than they did due to a thinner layer of sediment being present. Appendix B summarizes the results of a heuristic study that was conducted to estimate the timing and amplitude measurement accuracy of the filter used in this study.

In the current application, the input waveform used was an isolated direct-path arrival observed in the data for shot number 1 on the hydrophone at the shortest range. It was assumed that each shot will produce a similar waveform, so that a single spiking filter would suffice for all of the recorded data. The input wavelet is denoted by x_t and the spiking filter must re-shape this wavelet into a short duration spike. Figure 2 shows the wavelet used as the input x_t in this analysis. The selected waveform was obtained from the hydrophone closest to the detonation and is 69 samples in length.

The choice of the desired output waveform, z, is somewhat arbitrary in this case. Various candidates included a narrow square-topped pulse, a Gaussian-shaped pulse, and a triangular pulse. All of these were tried with various durations. Since accurate timing measurements were required, the duration of the pulse had to be small and contain a recognizable feature in the output shape that would serve as a reference point in the timing measurements. A subjective choice was made that the triangular pulse with a duration of four samples (1, 0.75, 0.5, 0.25) provided the best combination of a high P value (performance measure, *cf.* Appendix A), a short duration, and a clearly recognizable feature (*i.e.*, the apex between the vertical leading edge and the linearly decreasing tail).

In practice, a number of zeroes are added to either end of the pulse z to make the total waveform length, $m + 1$, the same length as the input x_t. The delay of the pulse z refers to the numbers of zeroes prefixed to the z waveform. Searching for the best spiking filter with the triangular pulse shape amounts to computing P for various combinations of delay and total length of the filter, and then finding the length-delay combination that results in the highest P value. In the present case, a search of the parameter space over the region where the Toeplitz matrix was nonsingular determined that P was optimized for a filter length of 76 points and a delay of 51 samples.

Figure 3 shows the 76-point filter generated for the input waveform x and the output waveform z with a delay of 51 samples. The filter performance factor for this example is $P = 0.916$. Application of this filter to recorded shot data should result in an output time-series composed of recognizable triangular-shaped pulses superimposed on a noise background. Figure 4 shows a close-up of the result of applying the filter to the direct and surface-reflected arrivals

from two different shots. Note that the origins of the time-series in this plot are arbitrarily chosen for display purposes and that the samples correspond to intervals equal to 1/699.05 seconds. The upper curve of the figure shows the spiked output obtained by applying the optimal spiking filter to the data record, as seen by the hydrophone closest to the detonation, for shot number 1. The positive going spike corresponds to the arrival of the direct path signal, while the negative going spike corresponds to the arrival of the surface-reflected path signal. Note that the peak amplitude of the first spike is approximately 0.9 in good agreement with the value of P for this filter. The lower curve is the result of applying the optimal spiking filter to the data record for shot number 2 (note that the curve has been offset by -1 for clarity). The resulting spiked signals are of lower amplitude for the second shot since the receiving array has moved approximately 1.2 km further away from the source position than it was for the first shot. Note that for this second shot the filter output contains a higher noise level than for the first shot; however, the timing and amplitudes of the real arrivals are accurately measured. As the signals become weaker for successive shot detonations (recall that the ship is continuously moving away from the source), the triangular shape of the spike is harder to recognize and spurious spikes can approach amplitudes similar to that of the desired signals. In practice, stacking the spiked time-series for each hydrophone group in the array aids in the recognition of *real* arrivals and noise spikes.

II. REFLECTION COEFFICIENT ESTIMATION

The method for estimating the reflection coefficient is based on the measurement of the amplitudes and the time differences between arrivals associated with the direct path, surface-reflected path, and bottom-bounce paths. The time differences were determined by counting the number of samples between the peak values at the onset of the spiked arrivals. The triangular shape of the spike was clearly recognizable in many, but not all of the processed data. In those records where the spike shape was not easily distinguished, it was usually possible to recognize a local maximum near the expected arrival time, and the peak instant was recorded. In addition, the relative amplitudes of the arrivals were determined by measuring the peak spike amplitudes.

For each shot, measured time differences between the direct and surface-reflected arrivals were used to determine the source range by globally minimizing the sum of the squared difference between a modelled and measured arrival time difference on each array element [3]. The source range was then used to provide spherical spreading corrections that were applied to both the measured direct and bottom-reflected arrival amplitudes. The ratio of the corrected bottom reflection spike amplitude to the corrected direct path arrival amplitude was formed to provide an estimate of the reflection coefficient-versus-range. The ray-trace model was then used to convert the coefficient estimates at given ranges to reflection coefficient-vs-grazing angle. The reflection coefficient-versus-grazing angle information was then inverted to obtain the geoacoustic parameters [5,6].

III. RESULTS FROM WEDGEX DATA

This section presents some selected results of the application of spiking filters to the WEDGEX [2] field data, shows and describes the reflection coefficient-vs-grazing angle data, and presents the results from inverting the reflection coefficient data.

Figure 5 shows the results obtained from the application of the spiking filter to the second shot in the data set. In Fig. 5(a), the direct and surface-reflected arrivals are shown. Channel 31 corresponds to the hydrophone closest to the detonation and shows the earliest arrivals. Note that the direct path corresponds to the peak in the trace pointing to the right, while the opposite polarity surface-reflected arrival corresponds to the second peak in the trace and points to the left. The hydrophone corresponding to channel 0 is approximately 1200 m further from the detonation than the hydrophone corresponding to channel 31. Note the reduction in the relative amplitude of the spikes and the decreasing time separation between the arrivals. Figure 5(b) shows the spiked primary bottom-bounce return. The traces in this figure have been given a gain of 4 relative to the traces shown in part (a). The four main ray-arrivals can be identified in this figure, but the surface-bottom and bottom-surface reflected paths are difficult to untangle from each other. In this work, the main interest is on the bottom-reflected path. This arrival is easily identified as the positive spike in the time period 1.4–1.9 seconds. The amplitude of this bottom-reflected arrival is much smaller than the arrivals shown in part (a) of the figure, but it was possible to identify the arrival on almost all of the hydrophones for each of the pre-critical reflections.

Figure 6 shows the estimated sea-floor reflection coefficient obtained by forming the ratio of the spiked amplitudes of the bottom-bounce and direct arrivals corrected for spherical spreading loss. For the larger grazing angles a reasonably accurate reflection coefficient estimate is anticipated because the first bottom-bounce return is well separated from

other arrivals. As the grazing angle is reduced, a loss of accuracy can be expected due to the decreasing separation of bottom-bounce and sub-bottom arrivals.

In this particular application the direct and bottom-bounce arrivals were always well separated; unfortunately, multiple returns occur in the bottom interacting signals that are not always well separated from the primary bottom-reflected arrival. The interfering returns are primarily caused by reflections from a sub-surface layer varying in depth from 40 – 15 m as the point of observation moves up-slope. Fig. 7 is a sketch of the bottom and sub-surface reflector. The sub-bottom returns influence the estimation of the reflection coefficient by causing errors in the measurement of the primary bottom-reflected signal amplitude. Fortunately, over most of the sampled grazing angles the sub-bottom returns are quite weak and have only minimal and sporadic effects resulting in some scatter in the reflection coefficient. As the grazing angle is reduced, some dominant sub-bottom returns are noted and these returns are responsible for many of the anomalously large reflection coefficient values (*i.e.*, those greater than unity). This mostly occurs for the data from shot number 8, which was the shot at greatest range from the receivers and; hence, supplied the smallest grazing angle data.

Care was taken to exclude those arrivals where sub-bottom returns greatly influenced the results. One can generally tell when this is happening by observing two consistent spikes in the data approaching one another and merging as the range to the source increases for successive hydrophones in the array. It was fortunate that the current problem allowed the critical angle to be clearly delineated. Had the surficial sediment layer been thinner, the arrivals from sub-bottom reflections might have obscured the critical angle of the surficial sediments. This problem with separating arrivals will limit the applicability of this reflection coefficient estimation technique in some cases, but the use of spiking filters to aid in preliminary interpretation is still recommended due to the relative ease and simplicity of their use and the resolution benefits that are realized. It should be noted that the scatter in the reflection coefficients obtained in the current analysis with this technique is comparable to the scatter that results when other techniques are used.

The reflection coefficient data have been interpreted as being the result of energy returns from a region of the sea-floor with changing properties [3,2]. Figure 7 shows the bathymetry of the bottom, the probable extent of a sand filled slump area, and the regions of the bottom where primary reflections occur. Using a ray-trace model it was determined that the first four shots lead to bottom interactions not far from the 1500 m depth contour. The sudden increase in the reflection coefficient near 25° is interpreted as the result of having reached the critical angle for the sea-floor material in the slump region. Shots 5 to 8 result in bottom interactions further up the slope away from the slump area. The increase in the reflection coefficient below 20° is interpreted as being due to reaching the critical angle for the slope material. The timing of the returns from the primary sub-surface reflector indicates that the thickness of the sediment layer above is reducing as the observation point moves toward the shallower water.

Using two different inversion schemes [5,6], the reflection loss data were used to provide estimates of the geoacoustic parameters of the material in the canyon area and on the slope. The results from these two different inversion schemes were quite similar; however, there were some differences observed in the estimated shear speeds. In general, the shear wave velocity estimates are very uncertain and tend to be coupled with the attenuation values which we have taken to be 0.5 dB/λ [2] as the pre-critical reflection data are insensitive to attenuation. Data from shots 1 to 4 were used to estimate the geoacoustic properties of the deep water region where the grazing angles were larger, while data from shots 5 to 8 were used to estimate the geoacoustic properties for the slope region. The results are that in the canyon the compressional speed is approximately 1650 m/s with a density $\rho \approx 2.1$ g/cc and shear speed less than 300 m/s. On the slope, the compressional speed is 1530 m/s and the shear speed is (very approximate) 80 m/s. Estimating the density on the slope is more difficult than in the canyon, but it appears that a density of 1.5 g/cc would fit well with the observed data and agrees with the density found by other researchers [11] working nearby.

The solid curves in Figure 6 represent the reflection coefficient-vs-grazing angle computed using a fluid-solid interface calculation [12]. The upper curve was calculated using the values determined from shots 1 to 4 (*i.e.*,a water speed of 1485 m/s, a sediment compressional speed of 1650 m/s, a density of 2.1 g/cc, and a compressional attenuation of 0.5 dB/λ). The lower curve was calculated using the values determined from shots 5 to 8 (*i.e.*, a sediment compressional speed of 1530 m/s and a density of 1.5 g/cc). The upper curve fits the observed data at steep grazing angles reasonably well, while the lower curve fits the data well at the shallow grazing angles.

Both inversion schemes are particularly sensitive to the rapid increase in the reflection coefficient estimates near the critical angle. It is obvious that one should attempt to measure the reflection coefficient at angles close to the critical angle to obtain minimum uncertainty in the inversion results.

IV. CONCLUSIONS

With the aid of spiking filters the reflection coefficient-vs-grazing angle has been measured at a location near the continental margin off the west coast of Vancouver Island. An interpretation of the acoustic data from the WEDGEX trial has previously determined that the geoacoustic properties of the sea-floor are changing along the tow path [2,3]. The reflection coefficient data has been interpreted as being due to reflections from two different regions of the sea floor. The reflection coefficients were separated according to the bottom regions where the reflections occurred and inverted. The results are that in the slump region (see Fig. 7) the sediments have properties similar to sand, while on the slope region the sediment is very similar to that found further out to sea [11].

An introduction to the technique for computing spiking filters has been presented in Appendix A and the accuracy of the spiking filter method for estimating the bottom loss has been investigated in a heuristic study of timing and amplitude measurement accuracy summarized in Appendix B. The accuracy study indicates that potential problems do exist for this method of determining the bottom-loss. In particular, the existence of secondary arrivals that are highly overlapped with the primary arrival can produce erroneous results. This fact, may limit the applicability of the technique in thin sediment regions. However, spiking filters provide a very convenient way of reducing the confusion resulting from moderately overlapped arrivals in the data record, and provide a means for making accurate estimates of arrival times and amplitudes in many situations of interest in underwater acoustics.

---

[1] D.W. Craig and L. McKee, "High Performance Shipboard Acoustics Data Acquisition, Imaging" Sea Technology **31**(1), pp. 51–53, January (1990).

[2] G.J. Heard, D.J. Thomson, and G.H. Brooke, "Two-way PE versus upslope propagation," *Ocean Reverberation* Eds. D.D. Ellis, J.R. Preston, and H.G. Urban, pp. 247–252, Dordrecht: Kluwer Academic Publishers, (1993).

[3] G.J. Heard, "Array positioning, bathymetry, and geoacoustic parameter estimation in a wedge-shaped ocean environment" in Proceedings of Oceans'93, Victoria Conference Centre, Victoria, B.C. Canada, IEEE and Oceanic Engineering Society, Vol.I, pp. 427–432, 18–21 October (1993).

[4] G.J. Heard, "Application of spiking filters to arrival time and amplitude measurement of underwater acoustic signals" DREP TM94-112, Defence Research Establishment Pacific, Fleet Mail Office Esquimalt, British Columbia, Canada, V0S 1B0, 1994.

[5] N.R. Chapman, K. Stinson, S. Levy, J. Cabrera, D.W. Oldenburg, "Estimation of the Elastic Properties of Seafloor Sediments by Inversion of Precritical Reflection Data" IEEE J. of Oceanic Eng., **13**(4), pp. 215–221, October (1988).

[6] D.E. Hannay and N.R. Chapman, "Inversion of geoacoustic profiles in thin-sediment environments from ocean bottom reflection loss data", Proceedings of Oceans'93, **III**, pp. 381–386, Victoria, B.C., Canada, 18–21 October 1993.

[7] M.D. Collins and W.A. Kuperman, "Focalization: environmental focusing and source localization" J. Acoust. Soc. Am., **90**, pp. 1410–1422, September 1991.

[8] E.A. Robinson and S. Treitel, "*Geophysical signal analysis*" Englewood Cliffs, N.J.: Prentice-Hall, pp. 140–212 (1980).

[9] N.R. Chapman, "Source levels of shallow explosive charges" J. Acoust. Soc. Am., **84**(2), pp. 697–702, 1988.

[10] D.E. Hannay, "Estimation of geoacoustic parameters of the ocean bottom by inversion of reflection loss data" Master's Thesis, Department of Physics and Astronomy, University of Victoria, Victoria, B.C., Canada, 1995.

[11] M.K. Sen, L.N. Frazer, S. Mallick and N.R. Chapman, "Analysis of multipath sound propagation in the ocean near 49° N, 128° W" J. Acoust. Soc. Am., **83**, pp. 588–597, 1988.

[12] L.M. Brekhovskikh, "*Waves in Layered Media*" Academic Press, New York, 1960.

[13] B.D. Bornhold and J.V. Barrie, "Surficial sediments on the western Canadian continental shelf" Continental Shelf Research, **11**,(8-10), pp. 685–699, 1991.

[14] B.D. Bornhold (private communication).

APPENDIX A: SPIKING FILTERS

Spiking filters are a class of least-squares shaping filters that convert a given waveform of specific functional shape to a new waveform of shorter duration and generally with a different functional description. These filters are well known to the seismic community, but they are not in widespread use in underwater acoustics. This section provides a brief description of spiking filters, but does not provide a complete background. Interested readers are referred to Robinson and Treitel [8] for a more comprehensive introduction to the topic.

The spiking filters are designed by minimizing the expected value of the squared error, J, determined from the input waveform x_t (with $t = 1 \ldots n$) and the desired output waveform z_t,

$$J = \sum_{t=1}^{n} \left\{ \left(z_t - \sum_{i=0}^{m} f_i x_{t-i} \right)^2 \right\}, \tag{A1}$$

with respect to the $m + 1$ spiking filter coefficients f_i. The minimization of J leads to the normal equations [8]

$$\sum_{i=0}^{m} f_i \phi_{xx}(k-i) = \phi_{zx}(k), \tag{A2}$$

for $k = 0, 1, 2, ..., m$, where ϕ_{xx} is the Toeplitz autocorrelation matrix of the input waveform x, and ϕ_{zx} is the cross-correlation vector of z and x. The solution of the normal equations gives the filter coefficients.

The squared error J is also used to assess the performance of the filter. Robinson and Treitel [8] define the *normalized mean square error* as

$$E = 1 - \sum_{i=0}^{m} f_i \frac{\phi_{zx}(i)}{\phi_{zz}(0)}. \tag{A3}$$

The normalized error is then complemented to give $P = 1 - E$. This performance measure runs from zero to one, with a value of 0 indicating poor performance and a value of 1 indicating good performance. The problem of finding the optimum spiking filter involves searching for the filter that results in the maximum value of P. In general, the longer the filter the better the result, but a practical upper limit to the filter length occurs when the Toeplitz matrix ϕ_{xx} becomes ill-conditioned. Another factor affecting the value of P is the delay of the desired output pulse relative to the start of the input waveform. Qualitatively, the best filter performance is obtained when the delay of the output spike best matches the delay of energy delivery in the input waveform. For example, poor performance will result if the user attempts to create an output spike near the beginning of the output waveform when the input waveform is a maximum-delay waveform.

In spiking filter applications the specification of the desired output waveform shape may be explicitly defined by the case at hand or it may be somewhat arbitrary. If the user is seeking accurate timing measurements, then the desired output pulse will necessarily be of short duration and will need to possess a clearly recognizable feature that can be used as a reference point for the timing measurement. Robinson and Treitel [8] give examples of a step function with a linearly decaying trailing edge (called here for convenience, a triangular pulse), a narrow square-topped pulse, a broader square-topped pulse, and a Gaussian-shaped pulse. Guidelines on how to choose the nature of the output pulse are limited, but Robinson and Treitel [8] suggest that, intuitively, output pulses with spectra similar to that of the input waveform may perform best.

APPENDIX B: ACCURACY OF TIMING AND REFLECTION COEFFICIENT AMPLITUDE

This paper has shown the result of applying a spiking filter to the WEDGEX data and using the amplitudes of the spikes to estimate the sea-floor reflection coefficient. The question now arises as to how accurate are the estimates that have been obtained using the spiking filter method? In order to answer this question in at least a heuristic manner, a study using simulated waveforms with varying arrival separations, signal-to-noise ratios, bandwidths, and filter characteristics was carried out [4]. Results of this study are summarized here, to provide an indication of the accuracy of the results that have been obtained.

The accuracy of the spiking filter approach to range and bottom parameter estimation was investigated by generating realistic simulated data with known arrival time separations and amounts of added noise. The direct-path waveform shown in Fig. 2 was used as a model, $a(t)$, of a realistic acoustic arrival and the received time series were assumed to consist of delayed, scaled replicas of this model waveform. The simulated time series, $s(t)$, were given by

$$s(t) = a(t) - b \cdot a(t - \tau) + c \cdot n(t), \tag{B1}$$

where b is a constant (usually equal to 1) that controls the amplitude of a second arrival, τ is the delay of the second arrival relative to the primary arrival a, and $n(t)$ is a sampled, zero mean, unity variance, Gaussian-noise time-series whose amplitude is controlled by the constant c. The second arrival is multiplied by a negative value to simulate the phase change that occurs on reflection at the surface of the sea. Simulated data were generated for arrival separations

of 5–100 samples (*i.e.*, waveforms overlapping by as much as 93%, to being completely separated by a time interval of almost half of the waveform length), for signal-to-noise ratios of 3.5–13.2 dB, for $P = 0.67$ to 0.92, and for nominal bandwidths $\Delta f = 200$, 140, and 90 Hz.

To summarize the results of the simulation study it was found that timing measurements were relatively insensitive to changes in the signal-to-noise ratio, the P value, and the bandwidth (at least for the bandwidths that were considered; using a greatly reduced bandwidth might have produced more effect). In general, timing estimates were accurate to within one sampling period, although at low signal-to-noise (3.5 dB) and for signals overlapped more than 60% of their length, a decreased accuracy was noted (error of up to 4 time samples). These results imply that for the shorter range shots that give rise to well separated direct and surface-reflected arrivals, the source-receiver distance should be very accurately determined. As the propagation distance becomes greater, the separation of the arrivals will be decreased and the resulting range estimates should become less accurate. Fortunately, some increase in the absolute range error can usually be tolerated at the larger ranges as the relative error remains small.

The measured amplitudes were found to be more sensitive to degraded conditions than the timing measurements were. In general, for separations exceeding 43% of the length of waveform a (*i.e.*, $\tau \geq 0.43 \cdot \text{length}(a)$), the measured amplitude was proportional to the value of P and degraded with decreasing signal-to-noise ratio. When the input signal amplitude was 5 or more times the noise amplitude, then performance was basically equivalent to the noise free performance. For separations of less than 25% of the input waveform length (≈ 25 ms), the amplitude measurement was significantly in error.

In the WEDGEX experiment the direct path arrival and the bottom-reflected arrivals were always well separated; however, sub-bottom arrivals were not always well separated from the primary bottom-bounce arrival, and the surface-reflected arrival was not always well separated from the direct path arrival. The interference of additional arrivals can have significant impact on the measured amplitude of the primary arrival. These effects are believed to be the cause of the scatter in the reflection coefficient measurements shown in Fig. 6 and also the primary cause of the anomalous values greater than unity. In fact, the potential exists for creating the appearance of a false critical angle due to the effect of highly overlapped arrivals. However, in the present case, care was taken to exclude situations where sub-bottom arrivals were not separable from the primary bottom-reflection and the existence of two critical angle regions is believed to represent the actual bottom conditions based on the good agreement with the results of others [11] found for the slope material parameters and knowledge of the bottom materials obtained from Bornhold and Barrie [13], and Bornhold [14].

The heuristic analysis of the spiking filter accuracy has indicated that applications involving timing measurements only are robust, and likely to produce accurate results when the degree of signal overlap is less than 60% of the input waveform length. On the other hand, caution must be applied to applications that require the measurement of spike amplitudes. When the signal-to-noise ratio is greater than 10 dB and the overlap of the arrival waveforms is less than 57%, then the amplitude measurements can be confidently accepted. These conditions were met for the majority of the data obtained from the first 8 of the 11 shots in the WEDGEX data set. Shot number 8 presented the majority of the difficulties in the data used in this paper due to the presence of a sub-bottom reflection that became inseparable from the bottom bounce reflection.

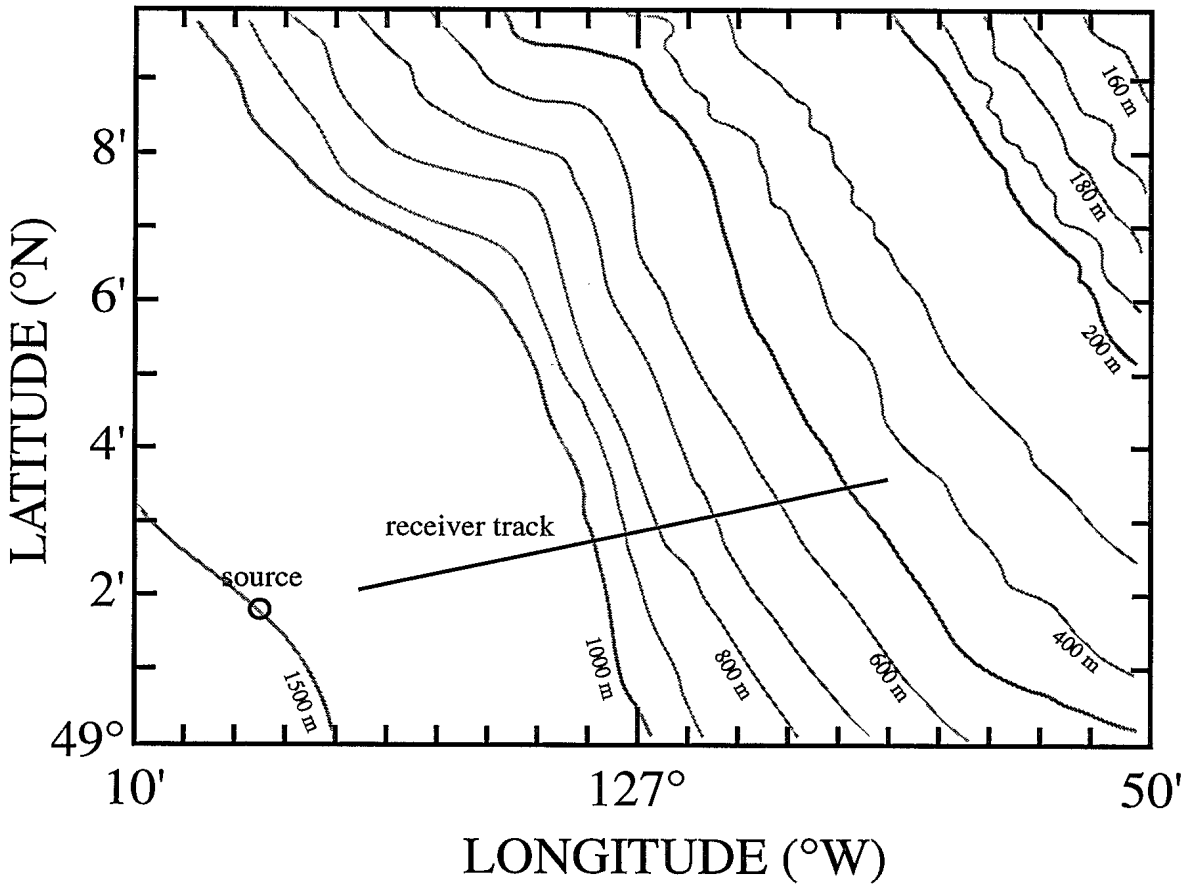

FIG. 1. The source location, receiver track, and bathymetry at the experiment site.

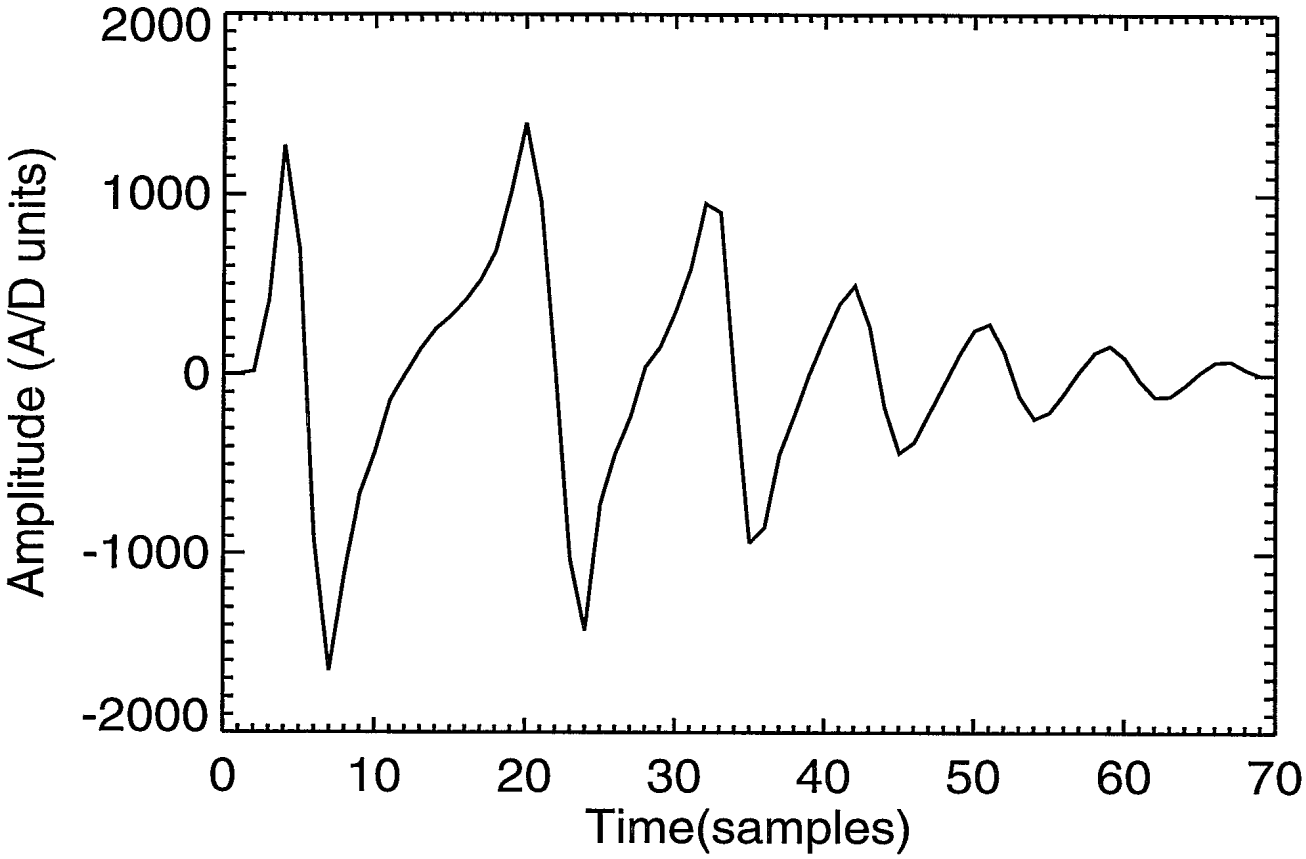

FIG. 2. Resolved direct-path arrival obtained from first shot detonation. This waveform was used as the input waveform x in the spiking filter normal equations.

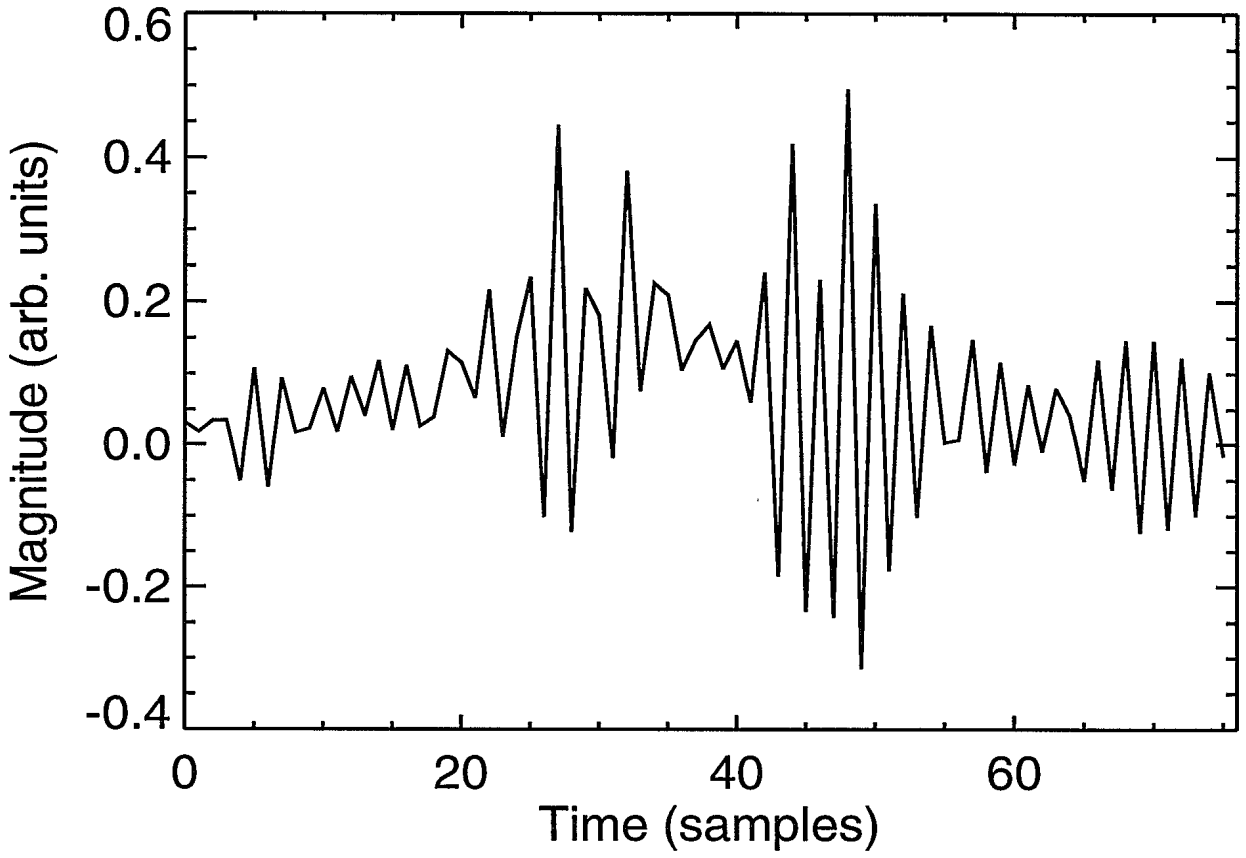

FIG. 3. A near optimal spiking filter for the isolated direct-path arrival of the SUS energy. For this filter $P = 0.916$, the length is 76 points, and the output delay is 51 samples.

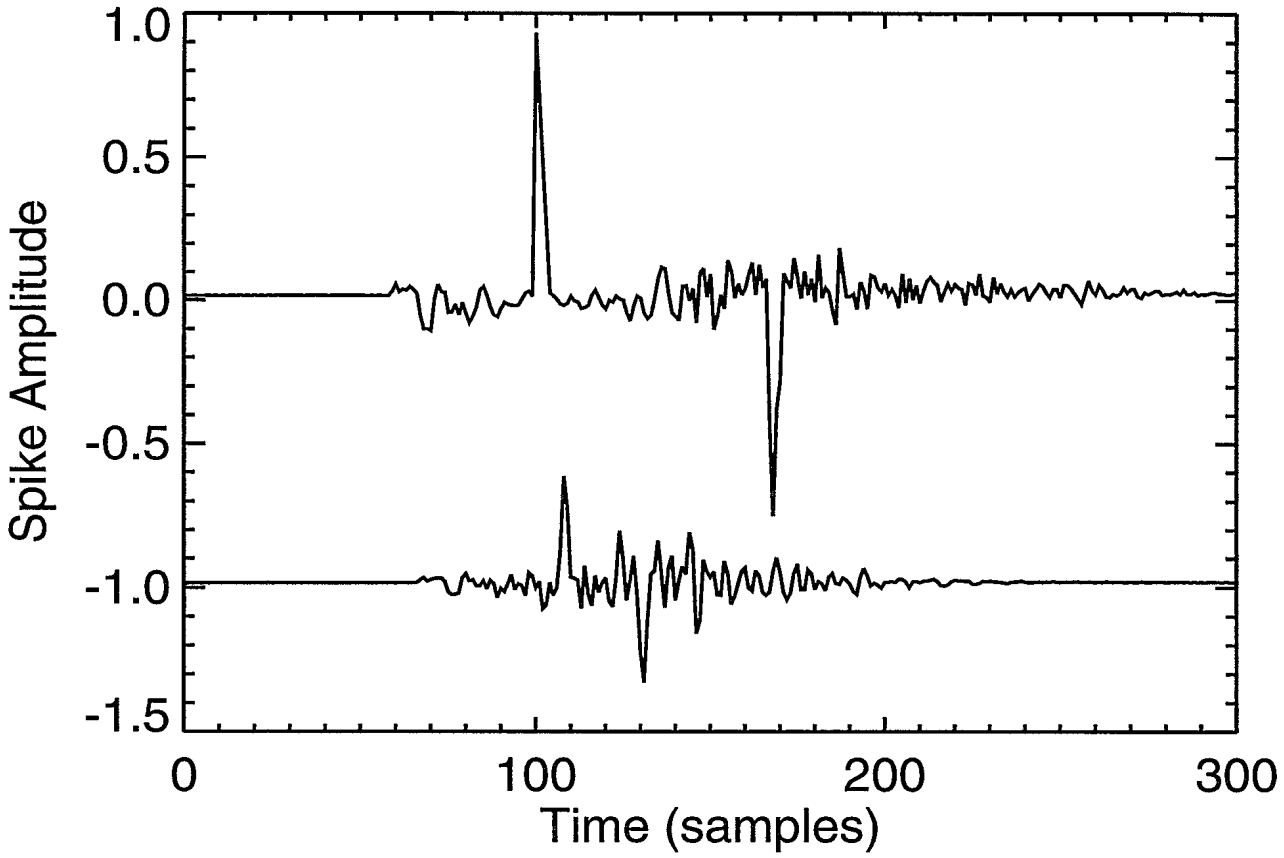

FIG. 4. The result of applying the filter in Fig. 3 to the direct and surface-reflected path arrivals from two different shot records. The lower curve has been offset by -1.

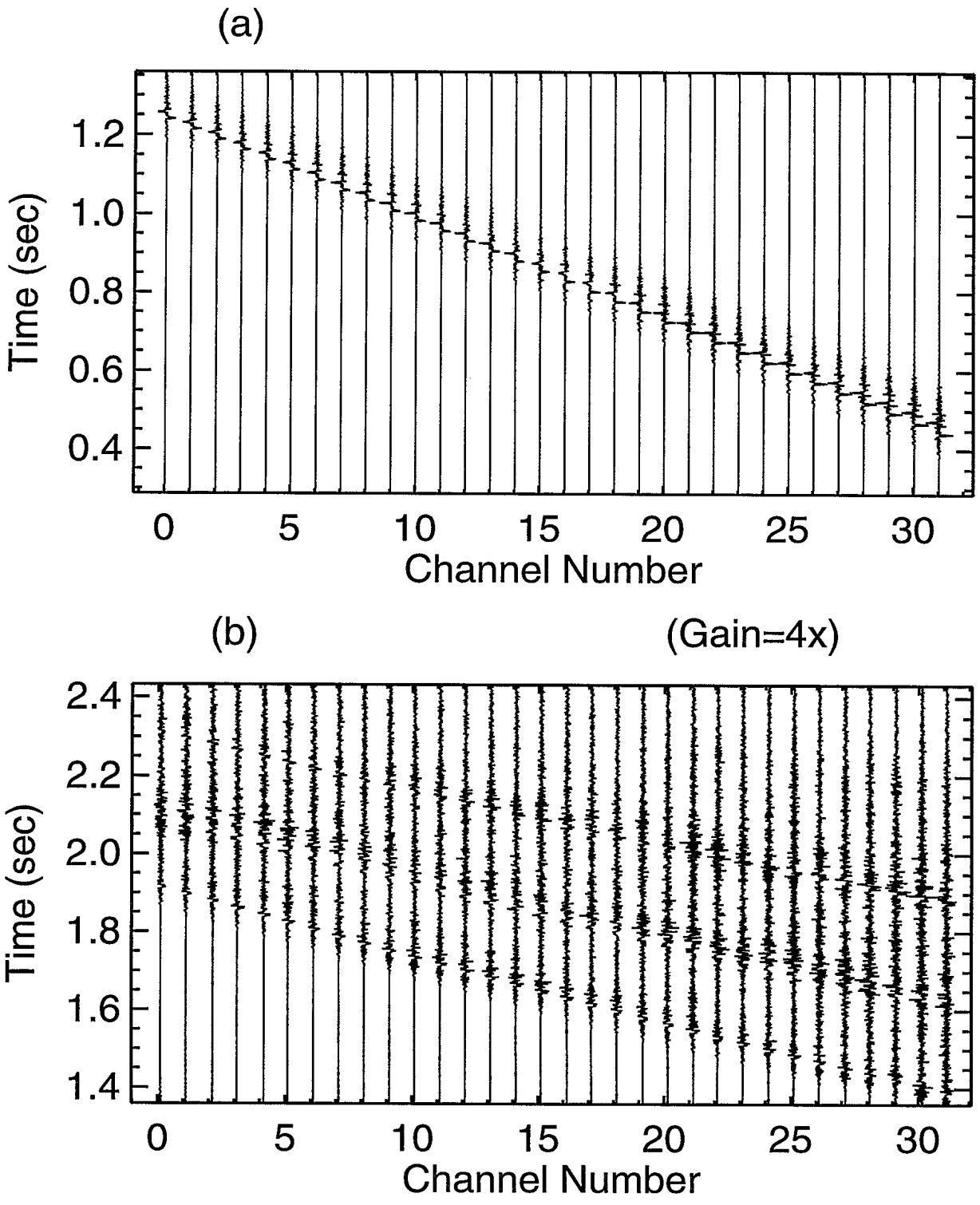

FIG. 5. The result of applying the filter in Fig. 3 to the data obtained from shot number 2. Each trace corresponds to one of 32 hydrophones in the receiving array. (a) The direct and surface-reflected arrivals and (b) first bottom-bounce arrivals.

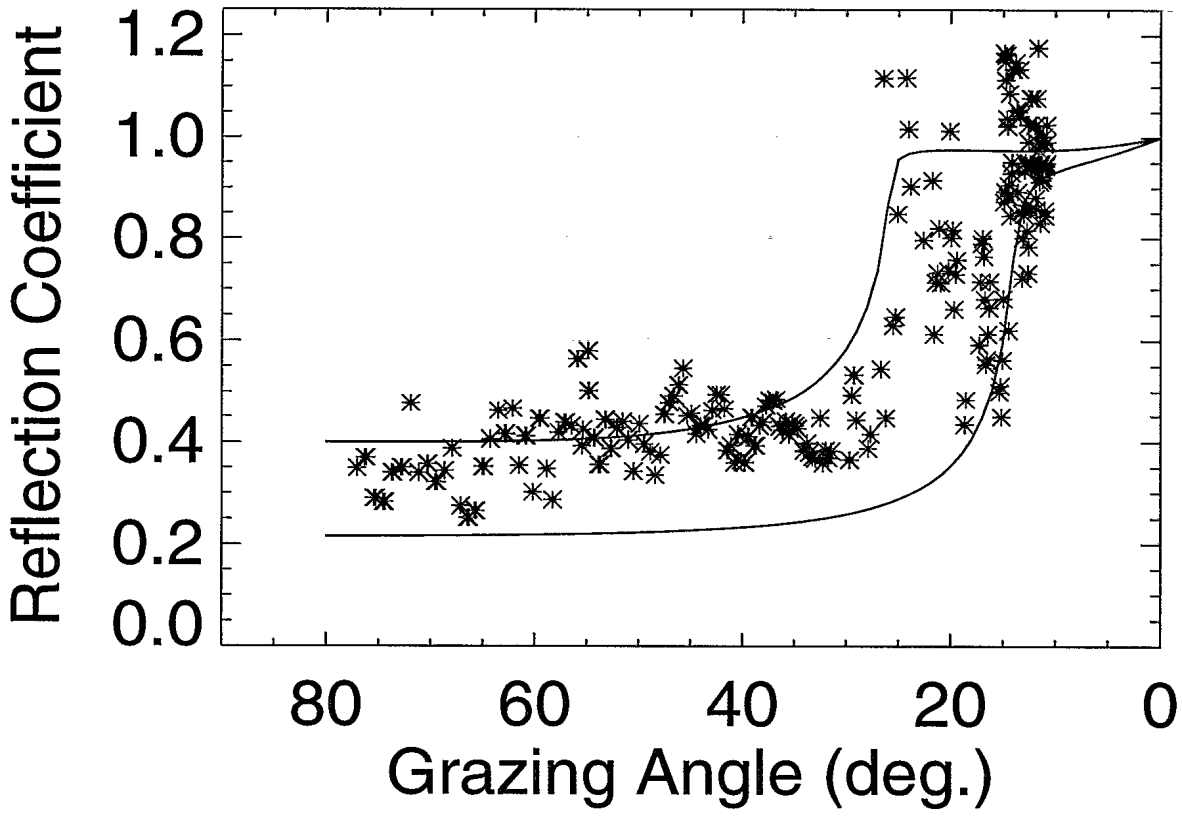

FIG. 6. Sea-floor reflection coefficient estimates obtained from the ratio of the direct and bottom-reflected spiked arrival amplitudes. Solid curves represent the computed reflection coefficients using the geoacoustic parameters obtained by inversion.

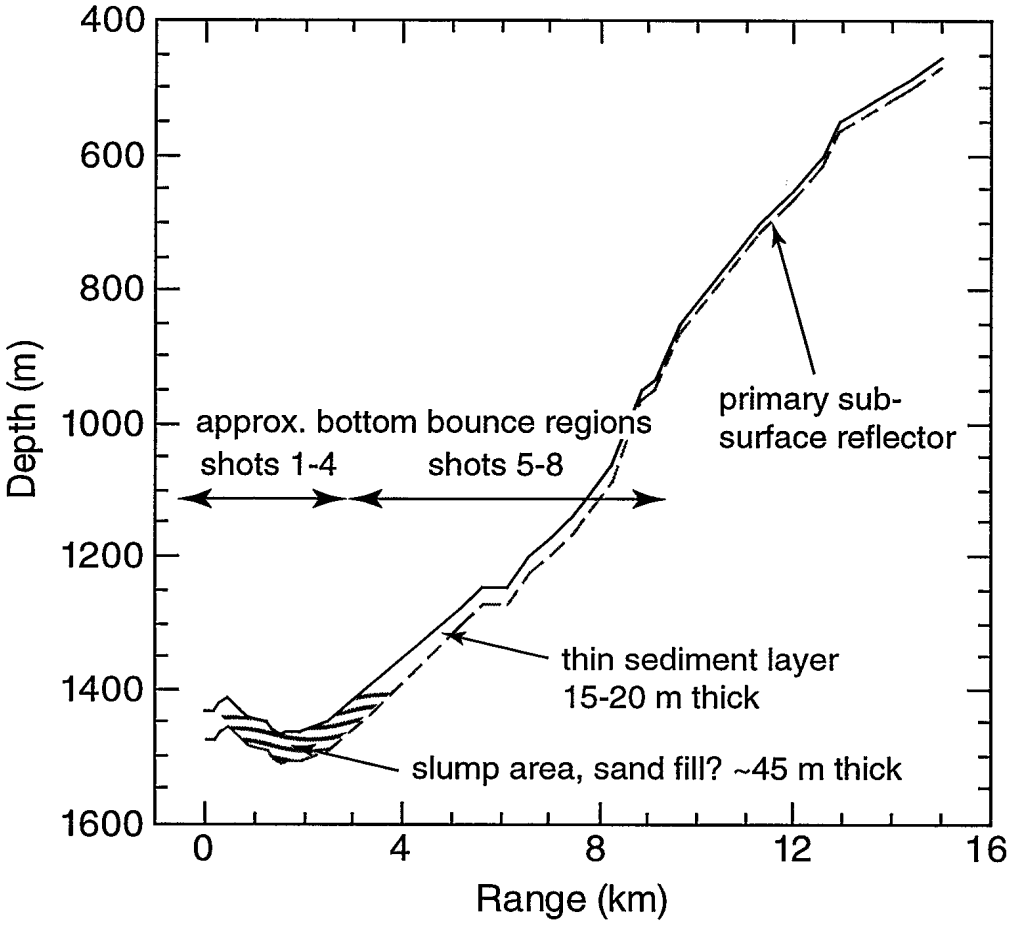

FIG. 7. Sketch of the bathymetry (dark line), primary sub-bottom reflector (dashed line), slump area, and reflection regions.

#501055